ナルの活性化が指摘されており，NHE1の活性化そのものが心肥大・心不全の直接的原因になり得るのか，またNHE1を介した関連シグナルの詳細は明らかでなかった。これらを解明するため，NHE1分子内の阻害ドメインを欠失した恒常的活性化型変異体を心筋特異的に高発現させたTgマウスを作製した。Tgマウスは予測どおり心肥大を呈し，やがて拡張型心筋症による心機能不全を起こしたが，これら病態はカリポライドで軽減された。細胞レベルでは，pH_i，Na^+濃度の上昇の他，$[Ca^{2+}]_i$の上昇，筋小胞体のCa^{2+}ハンドリング異常が起こり，これらが細胞死および心肥大シグナル活性化の引き金となることが予測された。生化学的解析により，NHE1による心肥大誘発経路としては主にCaMK II依存性シグナルが関与していることが分かった（投稿中）。

以上の結果は，NHE1の活性化が心肥大・心不全を発症するのに十分であり，NHE1がこれらの病態を起こすシグナル伝達の重要な一員であることを強く示唆している。

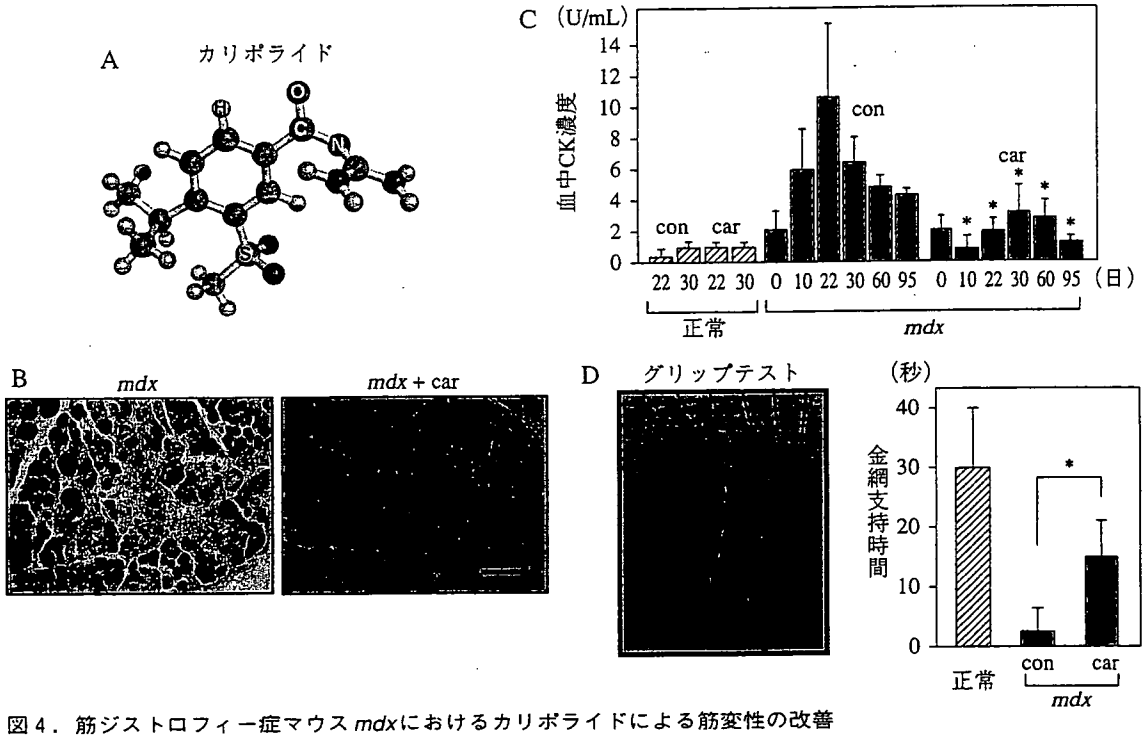

図4．筋ジストロフィー症マウス*mdx*におけるカリポライドによる筋変性の改善

A：カリポライドの化学構造．

B：*mdx*マウスにカリポライドを経口投与（3週間）すると骨格筋変性の著明な改善が見られた．ヘマトキシリン/エオジン染色．スケールは100μm．

C：筋変性のマーカーとしての血中クレアチンキナーゼ濃度変化．50日齢の正常および*mdx*マウスにカリポライド（car）を含む水を与えた．横軸は投与日数を示す．

D：グリップテストによる筋機能評価．*mdx*マウスにカリポライドを経口投与（3週間）すると金網支持時間に対する有意な改善効果が見られた．

Ⅲ. NHEと筋ジストロフィー

筋ジストロフィー(筋ジス)とは，筋線維の破壊・変性と再生を繰り返しながら，次第に筋萎縮と筋力低下が進行していく遺伝性筋疾患の総称である。発症年齢や遺伝形式，臨床的経過等から様々な病型に分類されるが，最も頻度の高いのはデュシェンヌ型筋ジストロフィー(DMD)であり，1987年に細胞骨格蛋白質であるジストロフィンがその原因遺伝子として特定された。DMD以外にも細胞骨格系蛋白質の異常に起因する筋ジスが数多く知られているが，未だ筋細胞変性の詳しい分子メカニズムは明らかでなく，良い治療法がないのが現状である。

著者らはジストロフィン欠損で筋ジスを発症するマウス(*mdx*)またはその関連蛋白質サルコグリカン欠損で筋ジスと心筋症を同時発症するハムスター(BIO14.6)をモデル動物として使用し，筋変性に効果的な薬の探索を行ってきた[17]。最近，NHEの阻害剤(カリポライドあるいはEIPA，化学構造は図4A参照)が筋変性に対して有効であることが分かってきた[18]。NHE阻害剤投与群では非投与群に比べて筋変性の指標となる血中クレアチンキナーゼ(CK)活性の有意な減少と組織ヘマトキシリン/エオジン染色で観察される筋変性の改善が認められた(図4B，C)。また，金網にマウスをぶらさがらせ，前足による体重支持時間を測定し，骨格筋の機能的評価(グリップテスト)を行ったところ，NHE阻害剤投与群において筋機能改善が示された(図4D)。このようなNHE阻害剤による筋変性の改善効果から，筋ジス筋ではNHEが活性化されており$[Na^+]_i$の上昇によって，前節で述べたようなNa^+依存性Ca^{2+}過負荷が起こり，筋変性が引き起こされる可能性が考えられた[18]。

そこで実際に筋ジス動物から調製した筋細胞を用いて，NHE阻害剤の筋変性保護メカニズムを検討した。筋細胞へのNa^+取り込み実験を行ったところ，全Na^+取り込みの大部分(65％以上)がNHEの特異的阻害剤で抑制されたことにより筋細胞におけるNa^+流入にNHEの寄与が大きいこと，そしてNHEを介する流入が筋ジス筋細胞で上昇していることが判明した。また筋ジス筋細胞では，コントロールに比べてpH_iの上昇，NHE活性のpH_i感受性の増加が観察された。$[Na^+]_i$も筋ジス筋細胞で約1.5倍上昇しており，カリポライド処理でコントロールレベルにまで減少した(図5A)。

以上の結果から，筋ジス筋細胞ではNHE活性が大幅に上昇していることが判明した。筋ジス筋細胞では外液Ca^{2+}濃度を上げるとコントロールでは観察されない$[Ca^{2+}]_i$の上昇が認められるが，この上昇はカリポライドであらかじめ処理することにより抑制され(図5B)，また同じ処理により伸展刺激による筋ジス筋細胞からのCK漏出も抑制された。この$[Ca^{2+}]_i$の上昇には強い外液Na^+濃度依存性があること，NCXブロッカーKB-R7943によって阻害されることから，筋ジス筋細胞ではNHEの恒常的な活性化による$[Na^+]_i$上昇がNCX活性を変化させることにより$[Ca^{2+}]_i$上昇をもたらし，筋変性につながることが示唆された[18]。

NHEの活性化はホルモン，機械刺激などで引き起こされる。筋ジス筋細胞におけるNHE活性化に寄与するいくつかの候補の中から，最近ATPが有力なメディエータになると考えられる以下の知見を得た[18]。①筋ジス筋細胞では，ATPの外液への遊離が未刺激時から確認され，伸展刺激によってさらにコントロールの2倍以上になることが分かった(図5C)。②ATP刺激でコントロール筋細胞ではNHE活性が上昇するが，筋ジス筋細胞ではNHEの恒常的活性化のためさらなる

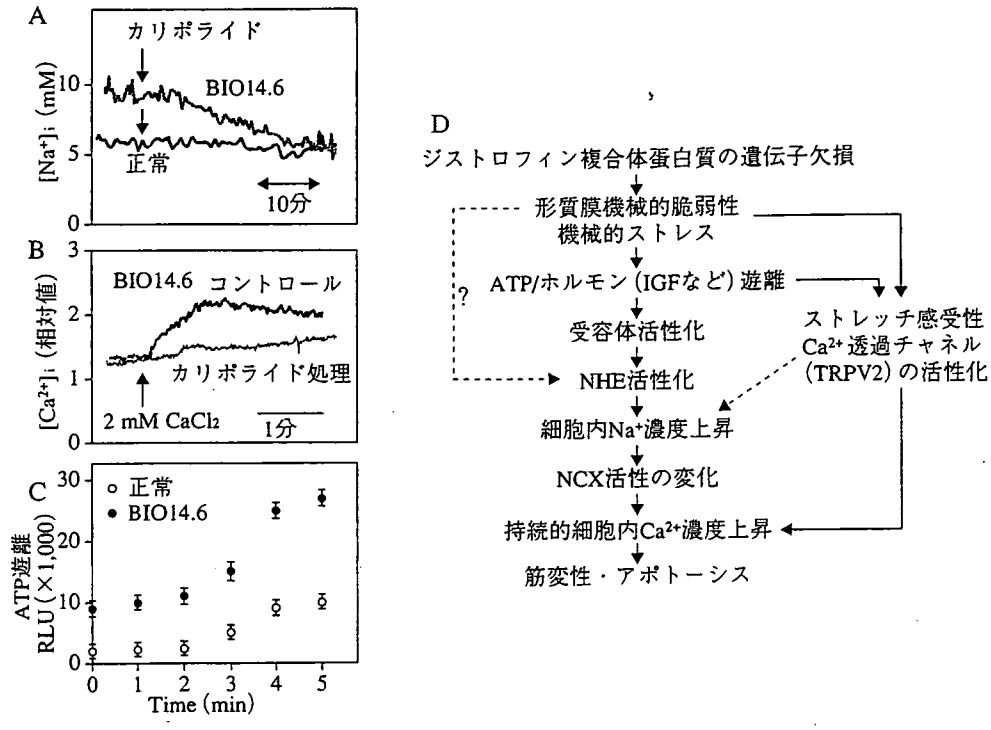

図5．筋ジスハムスター(BIO14.6)筋細胞を用いた筋変性の分子メカニズム
A：蛍光色素SBFIを用いて測定した$[Na^+]_i$はBIO14.6の細胞では高く，カリポライドで抑制される．
B：蛍光色素fluo4を用いて測定した$[Ca^{2+}]_i$．BIO14.6筋細胞では正常筋細胞では観察されない外液Ca^{2+}依存の$[Ca^{2+}]_i$上昇が見られるが，あらかじめカリポライド処理しておくとその$[Ca^{2+}]_i$上昇が抑制される．
C：シリコン膜に培養した正常およびBIO14.6筋細胞に10％伸展刺激を横軸に示す時間与えた時遊離されるATP量を測定．BIO14.6細胞からの著明なATP遊離がある．
D：現在考えられる筋ジスハムスター(BIO14.6)における筋変性発症に関わる細胞内メカニズム．*mdx*マウスも同様のメカニズムで筋変性が引き起こされる可能性がある．

上昇はなかった。③ATP分解酵素(アピラーゼ)およびP2受容体の阻害剤(PPADS，スラミン)処理により筋ジス筋細胞で上昇していたpH_iが減少し，ストレッチ刺激によるCK漏出も抑制された。④実際，BIO14.6および*mdx*両筋ジスモデルにおいて，P2受容体の阻害剤を投与したところ，NHE阻害剤と同等以上の筋変性改善効果が得られた。興味深いことに，NHEとP2受容体の阻害剤を併用すると，さらに相加的な改善効果が見られた。

以上の結果を踏まえて，細胞骨格系蛋白質の遺伝子欠損によって筋変性が生じるまでの細胞内経路をまとめてみた(図5D)。ジストロフィン関連の細胞骨格系の遺伝子異常でまず筋細胞膜が機械的に脆弱になり，ストレッチ刺激が入った状態になると考えられる。その増加したストレッチ刺激は，何らかのメカニズムでATP(あるいはIGFなどのホルモン)を遊離させ，受容体を介してNHEを活性化する。ストレッチが直接NHEを活性化する

可能性もある。いずれにせよ活性化されたNHEは$[Na^+]_i$を上昇させ，NCX関与で$[Ca^{2+}]_i$が上昇し筋変性を導く。他方，著者らは以前にストレッチ感受性Ca^{2+}透過チャネルTRPV2が筋変性に伴って活性化され，$[Ca^{2+}]_i$上昇に寄与することを報告した[9]。すなわち，TRPV2によるCa^{2+}流入系の亢進とNCXによるCa^{2+}排出系抑制の相乗効果が持続的な$[Ca^{2+}]_i$上昇に寄与することは疑いない。ジストロフィンあるいはサルコグリカンが欠損すると，骨格筋だけでなく心筋でも筋変性が起こり，移植しか治療の手段がない拡張型心筋症を発症する。心筋症における筋変性も筋ジスの骨格筋で解析したようなメカニズムの関与が考えられ，現在，治療薬開発への応用を検討している。

おわりに

本稿では，NHEは疾病を悪化させるいわば“悪玉”トランスポータとして紹介したが，KOマウスのフェノタイプを見ても明らかなように生理的には重要な蛋白質である。NHE(NHE1アイソフォーム)遺伝子を欠損させると，生後まもなく歩行性運動失調症やてんかん性痙攣発作などの神経変性症状を呈し，離乳前に死亡するケースが多い。またKOマウス全身の成長は遅く，これはおそらくpH_iが細胞増殖に関わることと関係があるだろう。カリポライドなどのNHE阻害剤の心臓病患者を対象とした臨床評価では，必ずしも意図した効果は得られなかった。しかしNHEを完全に抑制することは，Na^+蓄積を阻害する一方で，酸排出という生理的に重要な機能をも抑制してしまうことになりかねない。したがって，NHEの基本的な機能を堅持しつつも，“NHEの活性化をブロックする薬”が有効かもしれない。そのためにはまず，NHE活性制御の分子メカニズムを解明することが先決で，その先に画期的な創薬が見えてくるに違いない。

§ 文 献

1) Wakabayashi S, Shigekawa M, Pouyssegur J : Molecular physiology of vertebrate Na^+/H^+ exchangers. Physiol Rev 1997;77:51-74.
2) Orlowski J, Grinstein S : Diversity of the mammalian sodium/proton exchanger SLC9 gene family. Pflugers Arch 2004;447:549-65.
3) Wakabayashi S, Fafournoux P, Sardet C, et al : The Na^+/H^+ antiporter cytoplasmic domain mediates growth factor signals and controls "H^+-sensing". Proc Natl Acad Sci USA 1992;89:2424-8.
4) Hisamitsu T, Ben Ammar Y, Nakamura TY, et al : Dimerization is crucial for the function of the Na^+/H^+ exchanger NHE1. Biochemistry 2006;45:13346-55.
5) Hisamitsu T, Pang T, Wakabayashi S, et al : Dimeric interaction between the cytoplasmic domains of the Na^+/H^+ exchanger NHE1 revealed by symmetrical intermolecular cross-linking and selective co-immunoprecipitation. Biochemistry 2004;43:11135-43.
6) Pang T, Hisamitsu T, Wakabayashi S, et al : Role of calcineurin B homologous protein in pH regulation by the Na^+/H^+ exchanger 1 : tightly bound Ca^{2+} ions as important structural elements. Biochemistry 2004;43:3628-36.
7) Pang T, Su X, Wakabayashi S, et al : Calcineurin homologous protein as an essential cofactor for Na^+/H^+ exchangers. J Biol Chem 2001;276:17367-72.
8) Pang T, Wakabayashi S, Shigekawa M : Expression of calcineurin B homologous protein 2 protects serum deprivation-induced cell death by serum-independent activation of Na^+/H^+ exchanger. J Biol Chem 2002;277:43771-7.
9) Ben Ammar Y, Takeda S, Hisamitsu T, et al : Crystal structure of CHP2 complexed with NHE1-cytosolic region and an implication for pH regulation. EMBO J 2006;25:2315-25.
10) Karmazyn M, Gan XT, Humphreys RA, et al : The myocardial Na^+-H^+ exchange : structure, regulation, and its role in heart disease. Circ Res 1999;85:777-86.
11) Karmazyn M, Sawyer M, Fliegel L : The Na^+/H^+ exchanger : a target for cardiac therapeutic intervention. Curr Drug Targets Cardiovasc Haematol Disord 2005;5:323-35.

12) Wang Y, Meyer JW, Ashraf M, et al : Mice with a null mutation in the NHE1 Na^+-H^+ exchanger are resistant to cardiac ischemia-reperfusion injury. Circ Res 2003;93:776-82.
13) Avkiran M, Marber MS : Na^+-H^+ exchange inhibitors for cardioprotective therapy : progress, problems and prospects. J Am Coll Cardiol 2002;39: 747-53.
14) Engelhardt S, Hein L, Keller U, et al : Inhibition of Na^+-H^+ exchange prevents hypertrophy, fibrosis, and heart failure in beta(1)-adrenergic receptor transgenic mice. Circ Res 2002;90:814-9.
15) Kilic A, Velic A, De Windt LJ, et al : Enhanced activity of the myocardial Na^+/H^+ exchanger NHE-1 contributes to cardiac remodeling in atrial natriuretic peptide receptor-deficient mice. Circulation 2005; 112:2307-17.
16) Heineke J, Molkentin JD : Regulation of cardiac hypertrophy by intracellular signalling pathways. Nat Rev Mol Cell Biol 2006;7:589-600.
17) Iwata Y, Katanosaka Y, Wakabayashi S, et al : Protective effects of Ca^{2+} handling drugs against abnormal Ca^{2+} homeostasis and cell damage in myopathic skeletal muscle cells. Biochem Pharmacol 2005;70: 740-51.
18) Iwata Y, Hisamitsu T, Wakabayashi S, et al : Enhanced Na^+/H^+ exchange activity contributes to the pathogenesis of muscular dystrophy via involvement of P2 receptors. Am J Pathol 2007, in press.
19) Iwata Y, Katanosaka Y, Shigekawa M, et al : A novel mechanism of myocyte degeneration involving the Ca^{2+}-permeable growth factor-regulated channel. J Cell Biol 2003;161:957-67.

Polymer Journal, Vol. 39, No. 10, pp. 1065–1070 (2007)

Synthesis of Sugar-Polysiloxane Hybrids Having Rigid Main-Chains and Formation of their Nano Aggregates

Koutarou BEPPU,[1] Yoshiro KANEKO,[1] Jun-ichi KADOKAWA,[1,†]
Hidezo MORI,[2] and Takehiro NISHIKAWA[2]

[1]*Department of Nano-structured & Advanced Materials, Graduate School of Science and Engineering, Kagoshima University, 1-21-40 Korimoto, Kagoshima 890-0065, Japan*
[2]*National Cardiovascular Center Research Institute, 5-7-1, Fujishirodai, Suita 565-8565, Japan*

(Received March 22, 2007; Accepted July 12, 2007; Published August 28, 2007)

ABSTRACT: We synthesized sugar-polysiloxane hybrids having rigid main-chains by reaction of sugar-lactones with amine-functionalized polysiloxane (**1**). Reaction of gluconolactone (**2**) with **1** was performed to obtain polysiloxane (**3**) having polyol moieties derived from glucose. This material has the regularly controlled higher-ordered structure in solid state such as the hexagonal phase. A hydrophilic sugar-polysiloxane hybrid (**5**) was prepared by reaction of lactobionolactone (**4**) with **1**. Furthermore, an amphiphilic sugar-polysiloxane hybrid (**8**) was synthesized by introduction of stearoyl groups in addition to sugar groups on the surface of **1**. The SEM image of the amphiphilic material **8** exhibited formation of nano aggregates having the particle diameters of *ca.* 50 nm in water.
[doi:10.1295/polymj.PJ2006268]
KEY WORDS Glycopolymer / Sugar-lactone / Polysiloxane / Amphiphilic / Hybrid / Nano Aggregate /

There has been a growing interest in sugar portions of the glycoproteins because of exhibiting to bind to carbohydrate-recognition proteins, toxins, viruses, and cells. It has been known that a molecular assembly formed from the sugar-residues in the living system expresses stronger recognition ability than that of a single sugar molecule. This, so-called multivalent or cluster effect, has become a principle in the design of artificial glycoconjugate ligands. Therefore, polymeric materials having such functional sugar-residues, *i.e.*, 'glycopolymer', have widely been investigated because these materials efficiently show the multivalent effect.[1] So far, a number of such glycopolymers have been synthesized, which are composed of various organic polymer main-chains combined with a variety of sugar side-chains.[2–6]

Inorganic polymers such as polysiloxanes have various of interesting properties, *e.g.*, high oxygen permeability, low toxicity, and biocompatibility, which are advantages as biomaterials. Therefore, sugar-polysiloxane hybrids would be expected to have a significant potential for biological applications. In previous study, synthesis of such sugar-inorganic hybrids, composed of polydimethylsiloxane main-chain has been reported.[7–10] Since the main-chain has relatively flexible nature, nanostructures of the hybrid materials have not been controlled well.

Based on the above viewpoints, we paid attention to amine-functionalized polysiloxanes[11,12] for the main-chain of new sugar-polysiloxane hybrids, which were prepared by sol-gel reaction of amine-functionalized organoalkoxysilanes in strong acid aqueous solutions. The materials have rigid structures and construct hexagonal phase in solid state, because their frameworks are Si-O-Si network structures derived from trifunctional organoalkoxysilane. Furthermore, the materials are soluble in water and have reactive amino groups on the surface. Their rigidity, solubility, and reactivity would be advantageous properties to controlling nanostructures and introduction of various functional groups on the surface, in addition to the general characteristics of the inorganic polymers.

In previous communication, we briefly reported simple preparation method for a rigid polysiloxane hybrid (**3**) having polyol moieties using the amine-functionalized polysiloxane (**1**) and gluconolactone (**2**) (Scheme 1).[13] Because the sugar lactones like **2** react with the amino groups without protection of the hydroxy groups, they are useful substrates for such the simple procedure to exclude multi-reaction steps. However, **2** was not suitable for preparation of materials containing the sugar substituents, because the ring-opened moieties like the side chain of **3** formed from **2** had no any sugar-residues. Therefore, we have been carrying out studies on the synthesis of sugar-functionalized polysiloxane hybrids using disaccharide-lactone such as lactobionolactone (**4**), because the existence of sugar-residues can be maintained in spite of opening the lactone ring of **4** by the reaction with **1**.

†To whom correspondence should be addressed (Tel: +81-99-285-7743, Fax: +81-99-285-3253, E-mail: kadokawa@eng.kagoshima-u.ac.jp).

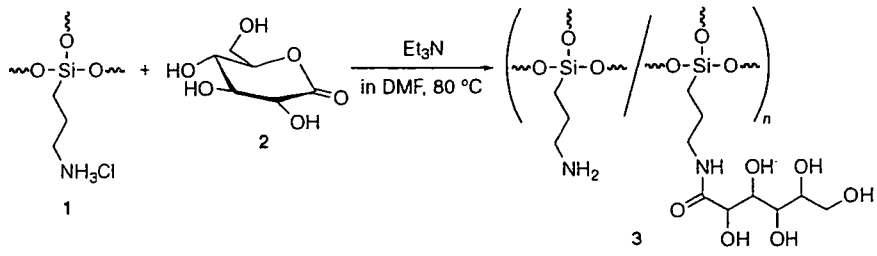

Scheme 1.

In this paper, we describe the synthesis of sugar-polysiloxane hybrids having rigid main-chains by the reaction of sugar-lactones with **1**. Furthermore, we prepared an amphiphilic sugar-polysiloxane hybrid by introduction of long alkyl chains in addition to sugar-residues on the surface of **1** to promote the formation of the nano aggregates in water, expecting the multivalent effects.

EXPERIMENTAL

Materials

The polysiloxane **1** was prepared according to the literature procedure.[11] *N,N*-Dimethylformamide (DMF), dimethyl sulfoxide (DMSO), and triethylamine were purified by distillation. Other reagents were used as received.

Reaction of 1 with Gluconolactone 2[13]

To a suspension of **1** (0.147 g, 1.0 mmol unit) in DMF (2.5 mL) was successively added triethylamine (0.15 mL, 1.1 mmol) and a solution of **2** (0.891 g, 5.0 mmol) in DMF (10 mL) with vigorously stirring at 80 °C under argon. After the mixture was stirred further at that temperature for 13 h, the obtained product was isolated by filtration, washed with DMF and acetone, and then dried under reduced pressure at 40 °C to yield 0.191 g of the yellow-powdered **3**. ^{1}H NMR (600 MHz, D_2O): δ 4.38–4.26 (br, -C(=O)-C*H*-), δ 4.16–4.05 (br, -C(=O)CH(OH)C*H*-), δ 3.88–3.60 (br, -C*H*(OH)C*H*(OH)CH_2-), δ 3.41–3.10 and 3.06–2.91 (br, -NCH_2-), δ 1.88–1.45 (br, -NCH$_2$CH_2-CH$_2$Si-), δ 0.94–0.47 (br, -CH_2Si-).

Synthesis of Hydrophilic Sugar-Polysiloxane Hybrid (5)

To a suspension of **1** (0.147 g, 1.0 mmol unit) in DMSO (3.0 mL) was successively added triethylamine (0.34 mL, 2.4 mmol) and a solution of **4** (1.701 g, 5.0 mmol) in DMSO (10 mL) with vigorously stirring at 80 °C under argon, and the mixture was stirred further at that temperature for 2 h. The mixture became gradually homogeneous solution. The solution was poured into acetone (300 mL) to precipitate the powdered product. The precipitated product was isolated by filtration, successively washed with acetone, hydrochloric acid (HCl) methanol solution and methanol, and then dried under reduced pressure at 40 °C to yield 0.332 g of the light yellow-powdered **5**. ^{1}H NMR (600 MHz, D_2O): δ 4.65–4.50 (br, -OC*H*-(CH-)O-), δ 4.50–4.32 (br, -C(=O)C*H*(OH)-), δ 4.32–4.13 (br, -C(=O)CH(OH)C*H*(OH)-), δ 4.08–3.49 (br, -C*H*(O-)C*H*(OH)CH_2OH, -C*H*(OH)C*H*(OH)C*H*(OH)-C*H*(O-)CH_2OH), δ 3.40–3.12 (br, -C(=O)NHCH_2-), δ 3.12–2.87 (br, Cl·NH$_3$CH_2-), δ 1.95–1.43 (br, -NCH$_2$CH_2CH$_2$Si-), δ 0.93–0.50 (br, -CH_2Si-).

Synthesis of Stearoyl-Carrying Polysiloxane (7)

To a solution of **1** (0.440 g, 3.0 mmol unit) in water (10 mL) was successively added triethylamine (1.0 mL, 7.2 mmol) and a solution of stearoyl chloride (**6**) (0.182 g, 0.6 mmol) in DMF (30 mL) with vigorously stirring at room temperature, and the solution was stirred further at that temperature for 10 min. After 5 mol/L HCl aqueous solution (2.88 mL, 14.4 mmol) was added to this mixture and this solution was stirred further for 5 min, the solution was poured into acetone (300 mL) to precipitate the powdered product. The precipitated product was isolated by filtration, washed with acetone and chloroform, and then dried under reduced pressure at 40 °C to yield 0.437 g of the white-powdered **7**. ^{1}H NMR (600 MHz, DMSO-d_6-D_2O): δ 3.09–2.72 (br, -NCH_2-), δ 2.20–2.01 (br, -C(=O)CH_2-), δ 1.88–1.55 (br, -NCH$_2$CH_2-CH$_2$Si-), δ 1.50–1.40 (br, -C(=O)CH$_2$CH_2-), δ 1.28–1.10 (br, -CCH_2C-), δ 0.95–0.45 (br, -CH$_3$, -CH_2Si-).

Synthesis of Amphiphilic Sugar-Polysiloxane Hybrid (8)

To a solution of **7** (0.150 g, 1.3 mmol unit) in DMSO (5 mL) was successively added triethylamine (0.46 mL, 3.3 mmol) and a solution of **4** (2.212 g, 6.5 mmol) in DMSO (15 mL) with stirring at 80 °C, and the solution was stirred further at that temperature for 2 h. The solution was poured into acetone (300 mL) to precipitate the powdered product. The precipitated product was isolated by filtration, successively washed with acetone, HCl methanol solution and

methanol, and then dried under reduced pressure at 40 °C to yield 0.270 g of the light yellow-powdered **8**. ^{1}H NMR (600 MHz, DMSO-d_6-D_2O): δ 4.46–4.28 (br, -OC*H*(CH-)O-), δ 4.28–4.11 (br, -C(=O)C*H*-(OH)-), δ 4.11–3.95 (br, -C(=O)CH(OH)C*H*(OH)-), δ 3.90–3.28 (br, -C*H*(O-)C*H*(OH)C*H*$_2$OH, -C*H*(OH)-C*H*(OH)C*H*(OH)C*H*(O-)C*H*$_2$OH, overlapped with HOD signal), δ 3.28–2.96 (br, -C(=O)NHC*H*$_2$-), δ 2.96–2.70 (br, Cl·NH$_3$C*H*$_2$-), δ 2.20–2.01 (br, -C(=O)-C*H*$_2$-), δ 1.80–1.32 (br, -NCH$_2$C*H*$_2$CH$_2$Si-, -C(=O)-CH$_2$C*H*$_2$-), δ 1.28–1.13 (br, -CC*H*$_2$C-), δ 0.88–0.80 (br, -CH$_3$), δ 0.80–0.36 (br, -C*H*$_2$Si-).

Measurements

The IR spectra were recorded using a SHIMADZU FT/IR-8400 spectrometer. The ^{1}H NMR spectra (600 MHz) were recorded using a JEOL ECA600 spectrometer. The gel permeation chromatographic (GPC) analyses were performed by using a TOSOH CCPD with RI detector under the following conditions: Shodex GF-310 column with water as the eluent at a flow rate of 0.5 mL/min. The calibration curve was obtained using pullulan standards. The X-ray diffraction (XRD) measurements were conducted at a scanning speed of $2\theta = 0.2°$/min using a RINT 1200 (Rigaku Co., Ltd) diffractometer with Ni-filtered CuKα radiation ($\lambda = 0.15418$ nm). The scanning electron microscope (SEM) images were obtained using a Hitachi S-4100 electron microscope. The dynamic light scattering (DLS) measurement was performed on a Zetasizer 3000 (Malvern Instruments).

RESULTS AND DISCUSSION

Reaction of 1 with 2

As previously reported,[13] an introduction of **2** to **1** was performed by heating at 80 °C in the presence of triethylamine in DMF to prepare a rigid polysiloxane **3** having polyol moieties (Scheme 1). The obtained product **3** was soluble in water and DMSO, but insoluble in typical organic solvents such as methanol, acetone, chloroform, and *n*-hexane.

The IR spectrum of the product showed an absorption at 1150 cm^{-1} attributed to the Si-O bond of the polysiloxane, an absorption at 1080 cm^{-1} assigned to the C-O bond of the polyol moiety derived from **2**, and an absorption at 1650 cm^{-1} due to the C=O bond of the amido group. In addition, the ^{1}H NMR spectrum in D_2O of the product showed both signals due to **1** and **2**. Furthermore, a methylene signal (δ 3.41–3.10) neighboring the amido group was appeared at lower magnetic field compared with a signal (δ 3.06–2.91) neighboring the unreacted amino group. These spectroscopic results indicated that the product has the structure **3** connecting **1** with **2** by the covalent bonds. The functionality of **2** to **1** was calculated to be *ca.* 75% based on the integrated ratio of the methylene signal neighboring the amido group to the methylene signal neighboring the silicon atom.

The molecular weights of **3** and **1** were evaluated by GPC analyses with water as the eluent. The GPC peak of **3** was shifted to the range of higher molecular weight compared to that of **1**. The M_n values of **3** and **1** estimated using pullulan standards were 21,200 g/mol ($M_w/M_n = 1.33$) and 10,300 g/mol ($M_w/M_n = 1.41$), respectively.

The XRD profile of **3** showed three peaks with the *d*-value ratio of $1:1/\sqrt{3}:1/2$ assigned to the (100), (110), and (200) peaks, respectively, indicating that the product has a hexagonal phase. Additionally, the *d*-value of the (100) peak of **3** ($d = 1.76$ nm) was larger than that of **1** ($d = 1.41$ nm). This indicates that the hexagonal phase in solid state was maintained in spite of the increase in the *d*-value by introduction of **2** to **1**.

The above analytical data indicated that **2** efficiently reacted with the amino groups in **1**, giving rise to **3**. To introduce the sugar moieties such as galactose residues on the surface of **1** by means of this reaction manner, the following experiments were performed using lactobionolactone **4**.

Synthesis of Hydrophilic Sugar-Polysiloxane Hybrid 5

We investigated synthesis of galactose-functionalized polysiloxane hybrid **5** by the reaction of **4** with **1**. Procedures for synthesis of **5** were almost same as those of **3**. Since the reaction in DMF gave the insoluble product, however, we employed DMSO as the alternative solvent, which was favorable for this reaction system. When an introduction of **4** to **1** was performed by heating at 80 °C in the presence of triethylamine in DMSO (Scheme 2), the initial reaction system was heterogeneous, which gradually became homogeneous with progress of the reaction. After the product was isolated as the fraction insoluble in acetone, unreacted amino groups were converted to ammonium cations by addition of HCl methanol solution in order to increase solubility and stability of the product in water. The obtained product **5** was soluble in water and DMSO, but insoluble in typical organic solvents such as methanol, acetone, chloroform, and *n*-hexane.

The IR spectrum of the product showed absorptions at 1650 cm^{-1} attributed to the C=O bond of the amido group, indicating the introduction of **4** to **1**. The ^{1}H NMR spectrum in D_2O of the product in Figure 1 shows both signals derived from **1** and **4**. Furthermore, a methylene signal $\mathbf{H_c}$ neighboring the amido group appeared at lower magnetic field compared with a signal $\mathbf{H_{c'}}$ neighboring the unreacted amino group. These spectroscopic data support the structure **5** of

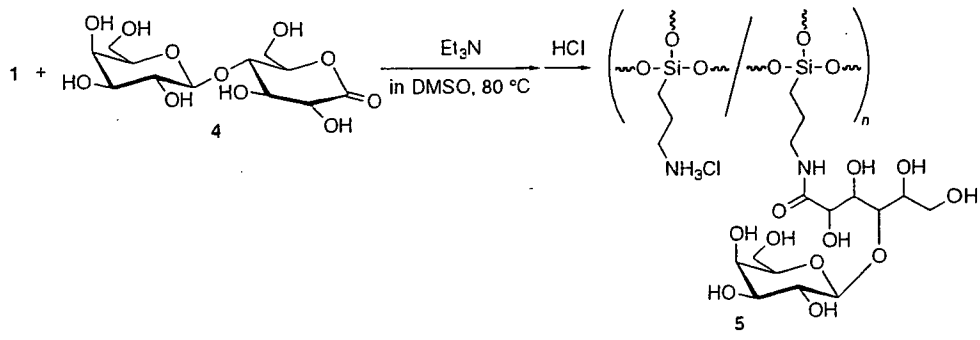

Scheme 2.

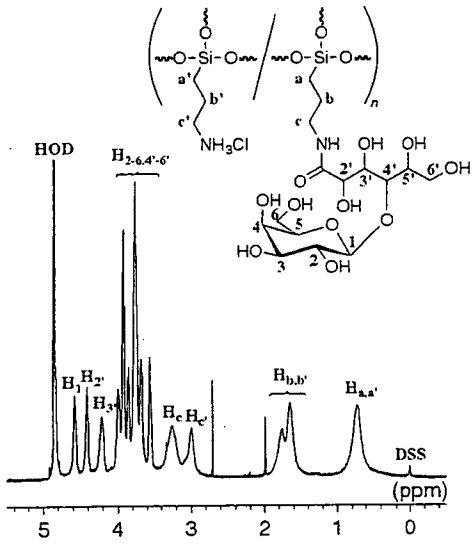

Figure 1. ^{1}H NMR spectrum of **5** in D_2O. Chemical shifts were referenced to sodium 2,2-dimethyl-2-silapentane-5-sulfonate (DSS) (δ 0.0 ppm).

the product. The functionality of **4** to **1** was calculated by the integrated ratio of the signal $\mathbf{H_1}$ to the signals $\mathbf{H_a}$ and $\mathbf{H_{a'}}$ in Figure 1 to be *ca.* 57%. Although the XRD profile of **3** showed three peaks for a typical hexagonal phase as described above, no diffraction peak was observed for **5**, indicating that a regular higher-ordered structure was not formed in the solid state. This would be because that the bulkiness of **4** affected the higher-ordered structure of **5**. However, **5** probably has the rigid structure in the solution due to the Si-O-Si network structure of the main-chain derived from trifunctional organoalkoxysilane. The molecular weight (M_n) of **5** estimated by GPC analysis with water as the eluent using pullulan standards was 44,700 g/mol (M_w/M_n = 1.44).

Synthesis of Amphiphilic Sugar-Polysiloxane Hybrid 8

To promote the formation of the nano aggregates of sugar-polysiloxane hybrid, we attempted synthesis of an amphiphilic hybrid **8** by introduction of the hydrophobic stearoyl groups in addition to the hydrophilic sugar groups on the surface of **5**. However, the reaction of **5** with stearoyl chloride **6** did not proceed to obtain **8**, probably due to bulkiness of sugar-residues existed on the surface of **5**. As an alternative reaction manner, an introduction of **6** to **1** was firstly carried out in the presence of triethylamine in water/DMF mixed solvent at room temperature to produce stearoyl-carrying polysiloxane **7** (Scheme 3). After addition of HCl aqueous solution to this reaction solution, the product was isolated as the fraction insoluble in acetone. The obtained product **7** was soluble in DMSO, but insoluble in water.

The IR spectrum of the product showed an absorption at 1640 cm^{-1} assigned to the C=O bond of the amido group. In addition, the ^{1}H NMR spectrum in DMSO-d_6 (including a small amount of D_2O) of the product in Figure 2 shows both signals derived from **1** and **6**. These spectroscopic results indicate the intro-

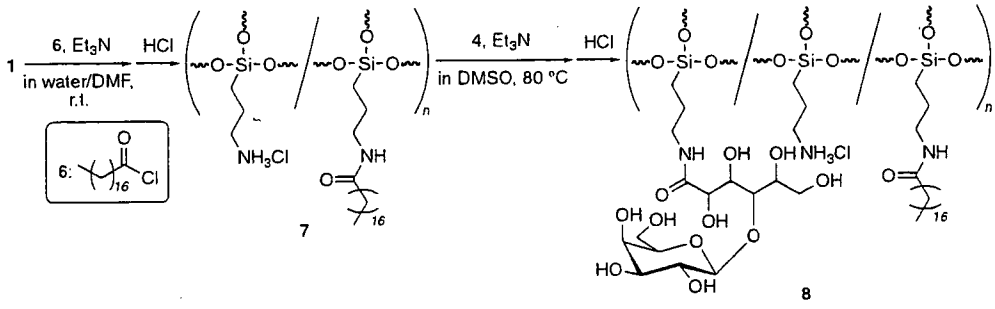

Scheme 3.

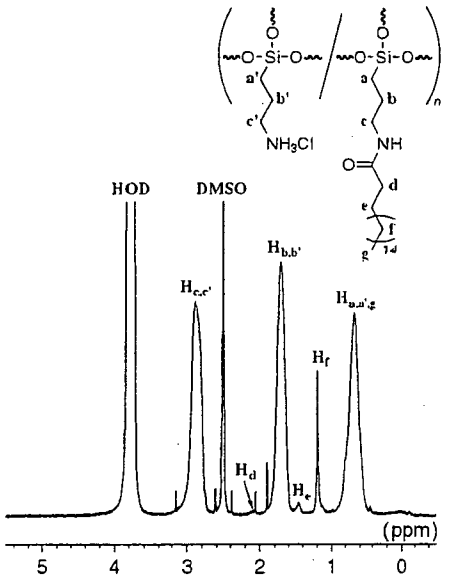

Figure 2. ^{1}H NMR spectrum of **7** in DMSO-d_6 (including a small amount of D_2O). Chemical shifts were referenced to DMSO (δ 2.5 ppm).

duction of **6** to **1**, leading to **7**. The functionality of **6** to **1** was calculated to be *ca.* 2% based on the integrated ratio of the signal $\mathbf{H_f}$ to the signal $\mathbf{H_b}$ and $\mathbf{H_{b'}}$. When the feed ratio of **6** to **1** was increased, the insoluble product was obtained.

As a second step, we carried out a reaction of **4** with **7** by heating at 80 °C in the presence of triethylamine in DMSO to obtain amphiphilic sugar-polysiloxane hybrid **8** (Scheme 3). The product was isolated as the fraction insoluble in acetone, followed by washing with acetone, HCl methanol solution, and methanol. The obtained product **8** was soluble in water and DMSO, but insoluble in typical organic solvents such as methanol, acetone, chloroform, and *n*-hexane.

The IR spectrum of the product showed an absorption at 1140 cm^{-1} attributed to the Si-O bond, an absorption at 1080 cm^{-1} assigned to the C-O bond of **4**, and an absorption at 1650 cm^{-1} due to the C=O bond of the amido group. Additionally, the ^{1}H NMR spectrum in DMSO-d_6 (including a small amount of D_2O) of the product in Figure 3a shows signals derived from **1**, **4**, and **6**. Furthermore, the methylene signals $\mathbf{H_a}$ and $\mathbf{H_b}$ of the product shift to higher field and the methylene signal $\mathbf{H_c}$ shifts to lower field compared with those of **7**. These shifts have also been observed in the synthesis of **3**,[13] and are attributed to progress of the amidation reaction of **7** with **4**. These spectroscopic results fully support the structure of the sugar- and stearoyl-functionalized polysiloxane **8**. The functionality of **4** to **1** was calculated by the integrated ratio of the signal $\mathbf{H_{f'}}$ to the signal $\mathbf{H_1}$ in Figure 3 to be *ca.* 48%, when the reaction was carried out under the conditions as described in experimental sec-

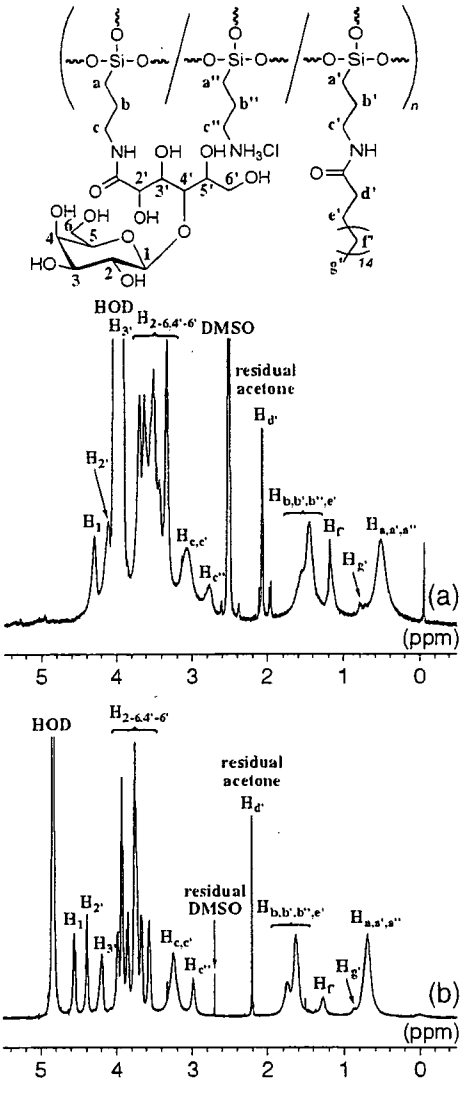

Figure 3. ^{1}H NMR spectrum of **8** (a) in DMSO-d_6 (including a small amount of D_2O) and (b) in D_2O. Chemical shifts were referenced to DMSO (δ 2.5 ppm) and DSS (δ 0.0 ppm), respectively.

tion. The functionalities were variable by changing the feed ratio of **4** to **7**.

Interestingly, intensity of a signal $\mathbf{H_{f'}}$ due to stearoyl group of **8** in D_2O decreases compared with that in DMSO-d_6 (Figure 3b). This observation indicates that the stearoyl groups existed in the inside of the intra and intermolecular aggregates of **8** in D_2O. To confirm the formation of nano aggregates of **8** in water, SEM image of **8** was taken. The SEM specimen was prepared by evaporating an aqueous solution of **8** on a spinning aluminium plate. The SEM image of the surface of **8** coated on the aluminum plate shows that nano aggregates were formed from **8** (Figure 4); nano aggregates having the particle diameters of *ca.* 50 nm are appearing at high frequency and larger particles that represent a diameter of *ca.* 500 nm are coexisting with smaller aggregates at much lower frequency (a few aggregates in a SEM image). The particle size

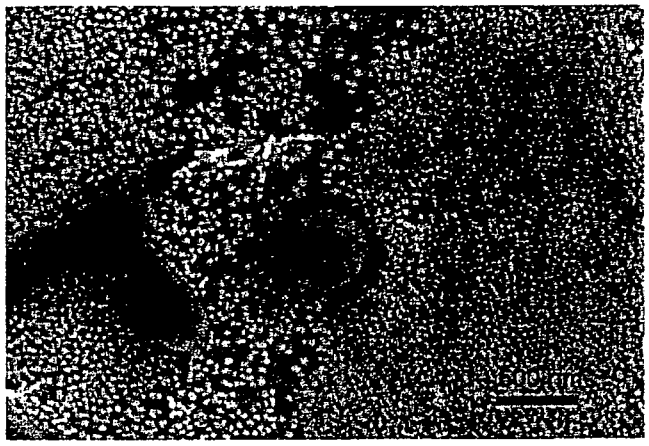

Figure 4. SEM image of **8**.

was also confirmed by dynamic light scattering (DLS) measurement. The mean diameter of the particle composed of **8** was 67.7 ± 4.5 nm (poly dispersity index: 0.273) in water. The aggregate size corresponds well to that was observed in the SEM image of the spin-coating sample of **8**.

CONCLUSIONS

The amino groups existed on the surface of the rigid polysiloxane (**1**) efficiently reacted with gluconolactone (**2**) to give the corresponding hybrid (**3**). This reaction manner was employed for preparation of the hydrophilic sugar-polysiloxane hybrid (**5**), which was achieved by the reaction of **1** with lactobionolactone (**4**). Furthermore, the amphiphilic sugar-polysiloxane hybrid (**8**) was also derived from **1** by the successive reactions with stearoyl chloride (**6**) and with **4**. The obtained hybrid materials **5** and **8** have galactose residues on their surfaces. Although hybrid **3** had the regular higher-ordered structure in the solid state, hydrophilic sugar-polysiloxane hybrid **5** did not form such a structure by the bulkiness of **4**. However, amphiphilic sugar-polysiloxane hybrid **8** formed the nano aggregates in water, which was confirmed by the ^{1}H NMR, SEM, and DLS analyses, expecting the multivalent effects of sugar-residues. The present materials are new class of sugar-inorganic hybrids, which have rigid polysiloxane main-chains.

Acknowledgment. The author (T.N.) thanks Dr. Tetsuji Yamaoka and Dr. Atsushi Mahara of National Cardiovascular Center for dynamic light scattering measurement.

REFERENCES

1. M. Okada, *Prog. Polym. Sci.*, **26**, 67 (2001).
2. K. Kobayashi, A. Tsuchida, T. Usui, and T. Akaike, *Macromolecules*, **30**, 2016 (1997).
3. X. L. Sun, K. M. Faucher, M. Houston, D. Grande, and E. L. Chaikof, *J. Am. Chem. Soc.*, **124**, 7258 (2002).
4. Q. Wang, J. S. Dordick, and R. J. Linhardt, *Chem. Mater.*, **14**, 3232 (2002).
5. A. B. Lowe, B. S. Sumerlin, and C. L. McCormick, *Polymer*, **44**, 6761 (2003).
6. L. Albertin, M. Stenzel, C. Barner-Kowollik, L. J. R. Foster, and T. P. Davis, *Macromolecules*, **37**, 7530 (2004).
7. G. Jonas and R. Stadler, *Acta. Polym.*, **45**, 14 (1994).
8. V. Braunmühl, G. Jonas, and R. Stadler, *Macromolecules*, **28**, 17 (1995).
9. V. Braunmühl and R. Stadler, *Polymer*, **39**, 1617 (1998).
10. K. Loos, G. Jonas, and R. Stadler, *Macromol. Chem. Phys.*, **202**, 3210 (2001).
11. Y. Kaneko, N. Iyi, K. Kurashima, T. Matsumoto, T. Fujita, and K. Kitamura, *Chem. Mater.*, **16**, 3417 (2004).
12. Y. Kaneko, N. Iyi, T. Matsumoto, and K. Kitamura, *Polymer*, **46**, 1828 (2005).
13. Y. Kaneko, J. Kadokawa, M. Setoguchi, and N. Iyi, *Polymer*, **46**, 8905 (2005).

ELSEVIER

NUTRITION

Nutrition 23 (2007) 81–86

www.elsevier.com/locate/nut

Basic nutritional investigation

Kurozu moromimatsu inhibits tumor growth of Lovo cells in a mouse model in vivo

Naoto Fukuyama, M.D., Ph.D.[a,*], Shio Jujo[a], Isao Ito, M.D., Ph.D.[b], Toru Shizuma, M.D., Ph.D.[a], Kazunori Myojin, M.D., Ph.D.[c], Kazuo Ishiwata, Ph.D.[a], Masanobu Nagano, Ph.D.[d], Hiroe Nakazawa, M.D., Ph.D.[a], and Hidezo Mori, M.D., Ph.D.[e]

[a] *Department of Physiology, Tokai University, School of Medicine, Isehara, Kanagawa, Japan*
[b] *Department of Surgery, Tokai University, School of Medicine, Isehara, Kanagawa, Japan*
[c] *Department of Radiology, Tokai University, School of Medicine, Isehara, Kanagawa, Japan*
[d] *Sakamoto Jozo Inc., Kagoshima, Kagoshima, Japan*
[e] *Department of Cardiac Physiology, National Cardiovascular Center, Suita, Osaka, Japan*

Manuscript received June 2, 2006; accepted October 12, 2006.

Abstract

Objective: In Japan, rice vinegar that has been matured and fermented for years in earthenware jars is considered a health food with anticolon cancer action. It is divided into the liquid component (Kurozu) and the sediment (Kurozu moromimatsu), which contains large amounts of organic materials and minerals. The effect of Kurozu moromimatsu (Kurozu-M) on cancer has not yet been examined. In this study, we examined the activity of Kurozu-M on colon cancer and investigated the mechanisms involved, focusing on active oxygen generation, apoptosis, and metalloproteinases (MMPs).

Methods: We used Lovo cells transplanted into nude mice as an experimental model. We measured the tumor volume and MMP levels and conducted hematoxylin-eosin staining (for polymorphonuclear leukocytes), terminal deoxynucleotidyl transferase-mediated dUTP nick end-labeling staining (for apoptosis), and immunostaining for nitrotyrosine (a marker of active oxygen generation) in control, Kurozu-treated, and Kurozu-M–treated groups.

Results: The tumor volume was the same in the control group (231 ± 36 mm^3) and Kurozu group (238 ± 52 mm^3), but was significantly reduced in the Kurozu-M group (152 ± 28 mm^3, $P < 0.001$ versus control). Apoptosis of tumor cells and accumulation of polymorphonuclear leukocytes were not observed. Nitrotyrosine production, total MMP levels, and MMP activation were significantly reduced in the Kurozu-M group.

Conclusion: The administration of Kurozu-M prolonged the lifespan of cancer cell–transplanted mice, inhibited tumor progression, and reduced nitrotyrosine production and MMP activation, but did not induce apoptosis.

Keywords: Kurozu; Kurozu moromimatsu; Lovo cell; Colon cancer

This work was supported by grants from Tokai University School of Medicine Research Aid in 2004, 2005, and 2006; the research and study program of Tokai University Educational System General Research Organization; the Kanagawa Nanbyou Foundation in 2004; Grants-in-Aid for Scientific Research in 2003 (grant 15659285), 2005 (grant 17659375), and 2006 (grant 18390336) from the Ministry of Education, Science and Culture, Japan; Health and Labour Sciences Research Grants for Research on Human Genome, Tissue Engineering Food Biotechnology in 2003 (grant H15-saisei-003); Health and Labour Sciences Research Grants for Comprehensive Research on Cardiovascular Diseases in 2004 (grant H16-jyunkannki[seishuu]-009) and 2006 (grant H18-jyunkannki[seishuu]-ippan-018); and Health and Labour Science Research Grants for research on medical devices for analyzing, supporting, and substituting the function of human body in 2005 (grant H17-physi-002).

* Corresponding author. Tel.: +81-463-931-121; fax: +81-463-936-684.
E-mail address: fukuyama@is.icc.u-tokai.ac.jp (N. Fukuyama).

0899-9007/07/$ – see front matter
doi:10.1016/j.nut.2006.10.004

Introduction

In Japan, rice vinegar is widely used in the preparation of Sushi or Kaisekiryouri. It is known to have a bactericidal action and an orexigenic action and was reported to have a preventive effect against hypertension and arterial sclerosis [1]. Recently, rice vinegar that has been matured and fermented for many years in earthenware jars has attracted attention as a health food. The supernatant is known as Korozu, and the solid residue of the production process, Kurozu moromimatsu (Kurozu-M), is rich in organic materials and minerals. However, the effect of Kurozu-M on disease has not yet been examined.

Colorectal cancer accounts for >90% of malignant tumors of the large intestine and is the third most common cause of death from malignant disease in the Western world [2]. It was reported that ethyl acetate extract of Kurozu inhibited carcinogenesis in azoxymethane-treated rats [3] and caused G0/G1 arrest through p21 induction in Caco-2 cells [4]. It is known that active oxygen species activate metalloproteinases (MMPs) in colon cancer tissue, leading to destruction of the basal membrane [5], thereby promoting distant metastasis. However, the effects of Kurozu on active oxygen production and MMP activation are unknown.

In this study, we examined the direct effects of Kurozu and Kurozu-M on human colon cancer cells (DLD cells, well-differentiated adenocarcinoma; Lovo cells, poorly differentiated adenocarcinoma) transplanted into nude mice and found that both inhibited tumor growth. We also examined the mechanisms involved, focusing on active oxygen production and MMP activation. Because direct measurement of active oxygen production in tissues is difficult, we used an indirect method based on staining for nitrotyrosine, the formation of which involves active oxygen.

Materials and methods

Preparation of Kurozu and Kurozu-M diets

The Kurozu and Kurozu-M diets were obtained from Sakamotojyozo Co., Ltd. (Kagoshima, Japan). The Kurozu diet included 0.32% 10-fold–concentrated Kurozu, and the Kurozu-M diet included 2% Kurozu moromimatsu powder in CE-2 basic rodent diet (Nihon CLEA Co., Ltd, Tokyo, Japan).

Preparation of animal model

Lovo and DLD cells were maintained under the conditions recommended by the supplier. Four-week-old to 6-wk-old female nude mice were maintained in a pathogen-free environment and handled according to the university's guidelines for animal care and use.

Female nu/nu mice were injected with 1×10^6 Lovo cells or DLD cells into the right flank. The tumors reached 5–10 mm in diameter at about 6 wk after injection in the control group on a standard CE-2 diet. The CE-2, Kurozu, or Kurozu-M diet was supplied from 1 wk before cancer cell injection.

Measurement of subcutaneous tumor

Tumor dimensions were measured with a linear caliper every 2 or 3 days for one month. We measured the major axis and the tumor volume, which was calculated using the equation $V\ (mm^3) = a \times b^2$, where a is the largest dimension and and b is the perpendicular diameter.

Hematoxylin-eosin staining, terminal deoxynucleotidyl transferase-mediated dUTP nick end-labeling staining, and nitrotyrosine immunostaining

At the end of the experiment, tumor tissue was fixed with 4% paraformaldehyde and sectioned. Hematoxylin-eosin (HE) staining was performed with conventional methods. Terminal deoxynucleotidyl transferase-mediated dUTP nick end-labeling (TUNEL) staining was performed according to the kit manufacturer's instructions, and apoptosis was visualized as brown staining, located in the nucleus. Apoptotic cells were counted in 10 fields of each slide under a 40× microscope.

For nitrotyrosine staining, endogenous peroxidase in sections was quenched with 0.3% H_2O_2 in 60% methanol for 30 min. The sections were permeabilized with 0.1% Triton X-100 in phosphate buffered saline (PBS) for 20 min. Nonspecific adsorption was minimized by incubating the sections in 2% normal goat serum in PBS for 20 min. Sections were incubated overnight with anti-nitrotyrosine rabbit polyclonal antibody (1:500 in PBS), and specific labeling was detected with diaminobenzidine tetrahydrochloride. To verify the binding specificity to nitrotyrosine, some sections were incubated with primary antibody only (no secondary antibody) or with secondary antibody only (no primary antibody). No positive staining was found in these sections, indicating that the immunoreaction was specific. Some sections were incubated with the primary antibody (anti-nitrotyrosine) in the presence of excess nitrotyrosine (10 mM) to further verify the binding specificity.

MMP-2 and MMP-9 assays

Levels of total MMP-2 and MMP-9 and endogenous activated MMP-2 and MMP-9 were assayed with commercial assay kits (Amersham Pharmacia Biotech, Buckinghamshire, UK).

MMP-2 assay

Eight weeks after injection of Lovo cells, tumors were removed. Tissues were homogenized in 50 mM Tris-HCl buffer (pH 7.4) containing 1 mM monothioglycerol and

centrifuged at 2000 *g* for 10 min. The supernatant was used as the sample. One hundred microliters of each standard blank or sample (in duplicate) was added to wells coated with MMP-2 antibody. The 96-well plate was then incubated overnight at 4°C. Any MMP-2 present within the samples was bound to the wells and other components were removed by washing. All standards and one well for each sample were activated with aminophenylmercuric acetate (APMA, 0.5 mM) to determine total MMP-2 levels, and the remaining wells were incubated with assay buffer alone to determine endogenous activated MMP-2. The detection reagent was then added to each well and the plate was incubated at 37°C for 4 h. After incubation, the absorbance of each well was read at 405 nm on a microplate reader and the concentrations (nanograms per milliliter) of total MMP-2 and endogenous activated MMP-2 were determined for each sample from a standard curve using Revelation Software (Dynatech, UK). Final tissue values were expressed as nanograms per milligram of protein.

MMP-9 assay

Standards and samples were run in the same manner as described for MMP-2 on a microplate coated with MMP-9 antibody, except that 1 mM APMA was used for activation, and incubation with the detection reagent was done at 37°C for 6 h. The absorbance was read with a microplate reader as described for MMP-2. Final tissue values were expressed as nanograms per milligram of protein.

Results

Measurement of subcutaneous tumor

We measured the major axis of the tumor to examine whether the administration of Kurozu or Kurozu-M could inhibit tumor growth. In the DLD cell–transplanted model, the major axes were 8.1 ± 0.5 mm in the control group, 7.90 ± 0.80 mm in Kurozu group, and 7.8 ± 0.80 mm in the Kurozu-M group. There were no significant differences among the three groups (Fig. 1A). However, in the Lovo cell–transplanted model, the major axes of the tumor were 8.2 ± 0.5 mm in the control group and 7.8 ± 0.8 mm in the Kurozu group, but significantly reduced to 6.0 ± 0.8 mm in the Kurozu-M group ($P < 0.05$ versus control; Fig. 1B).

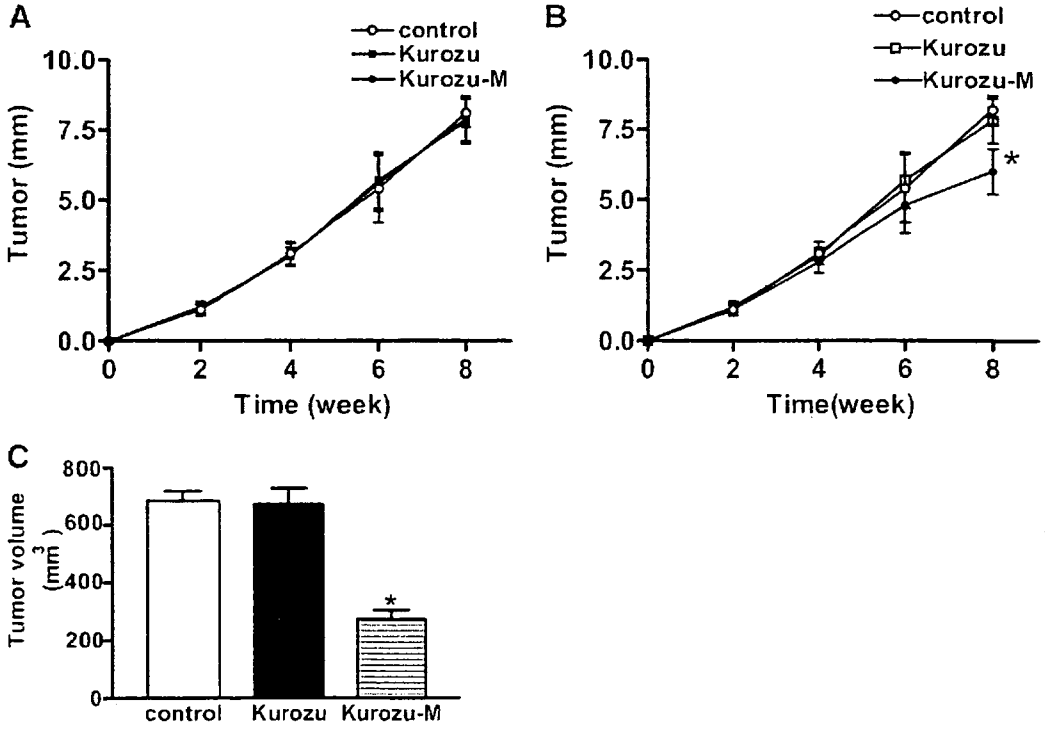

Fig. 1. Antitumor effect of Kurozu and Kurozu moromimatsu. Female nu/nu mice were injected with 1 × 10^6 Lovo cells or DLD cells into the right flank. (A) Time course of tumor growth in DLD-1 cell–transplanted mice (long diameter). Open circles represent the control group, solid squares the Kurozu-treated group, and solid circles the Kurozu moromimatsu–treated group. (B) Time course of tumor growth in Lovo cell–transplanted mice (long diameter). Open circles indicate the control group, open squares the Kurozu-treated group, and solid circles the Kurozu moromimatsu–treated group. (C) Tumor volume in Lovo cell–transplanted mice. Tumor volume was measured 8 wk after Lovo cell inoculation. The open bar indicates the control group, the solid bar the Kurozu-treated group, and the horizontally lined bar the Kurozu moromimatsu–treated group. Values are means ± SD. *$P < 0.001$ versus other groups.

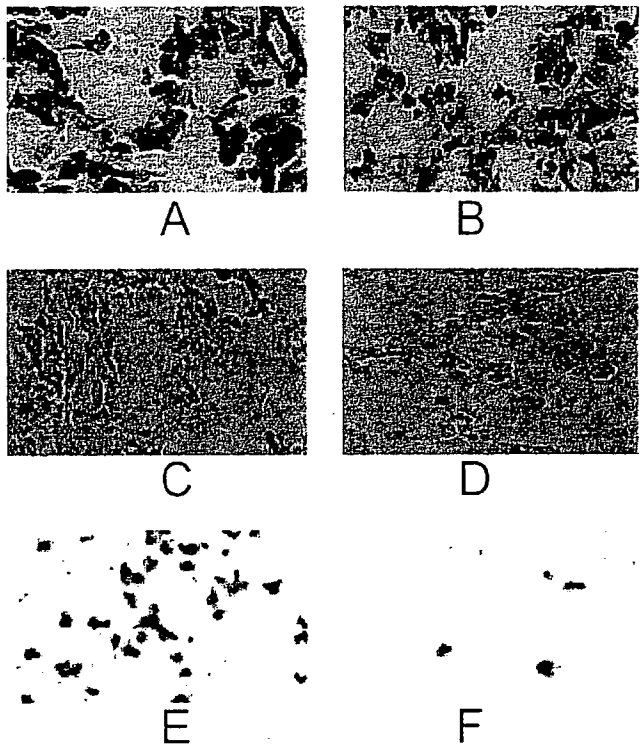

Fig. 2. Histologic examination of cancerous tissue after Lovo cell transplantation. Hematoxylin-eosin staining of tumor from (A) the control group and (B) the Kurozu moromimatsu–treated group. Terminal deoxynucleotidyl transferase-mediated dUTP nick end-labeling staining of tumor from (C) the control group and the (D) Kurozu moromimatsu–treated group. Nitrotyrosine staining of tumor from (E) the control group and (F) the Kurozu moromimatsu–treated group.

In the Lovo cell–transplanted model, the tumor volumes were 684.0 ± 34.0 mm^3 in the control group, 672.0 ± 56.0 mm^3 in the Kurozu group, and 273.0 ± 32.0 mm^3 in the Kurozu-M group ($P < 0.005$ for the Kurozu-M group versus control; Fig. 1C).

The following results refer to the Lovo cell–transplanted model.

HE staining, TUNEL staining, and nitrotyrosine immunostaining

The HE staining showed no accumulation of polymorphonuclear leukocytes, which have been implicated in active oxygen production, in tumor tissue in the control group or the Kurozu-M group (Fig. 2A,B).

The TUNEL staining indicated that apoptosis in the Kurozu-M group was at the same level as that in the control group (Fig. 2C,D).

Because we previously found that nitrotyrosine, generated from peroxynitrite and tyrosine, is produced in human colon cancer [5], we examined whether the administration of Kurozu-M could inhibit nitrotyrosine formation. In the control group, many cells produced nitrotyrosine, whereas in the Kurozu-M group, only a few cells produced nitrotyrosine (Fig. 2E,F).

MMP-2 and MMP-9 assays

To investigate the role of MMPs in the action of Kurozu-M, we examined whether or not Kurozu-M altered the levels and activation of MMPs.

Total MMP-2 amounted to 8.8 ± 2.5 ng/mg of protein in the control group and 8.6 ± 2.8 ng/mg of protein in the Kurozu group. However, it was significantly reduced to 5.6 ± 1.8 ng/mg of protein by administration of Kurozu-M ($P < 0.05$ versus control; Fig. 3A). Activated MMP-2 amounted to 0.25 ± 0.06 ng/mg of protein in the control group, 0.27 ± 0.08 ng/mg of protein in the Kurozu group, and 0.12 ± 0.05 ng/mg of protein in the Kurozu-M group ($P < 0.05$ for the Kurozu-M group versus control; Fig. 3A).

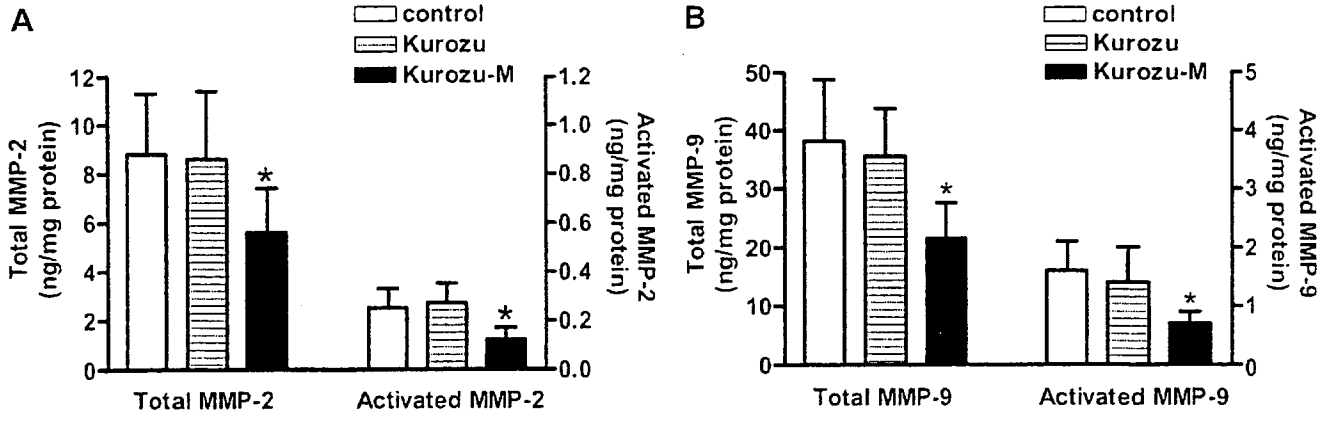

Fig. 3. Anti-metalloproteinase effect of Kurozu and Kurozu moromimatsu. (A) Total and activated metalloproteinase-2 in cancerous tissue after Lovo cell inoculation. The open bar represents the control group, the horizontally lined bar the Kurozu-treated group, and the solid bar the Kurozu moromimatsu-treated group. (B) Levels of total and activated metalloproteinase-9 in cancerous tissue after Lovo cell inoculation. The open bar represents the control group, the horizontally lined bar the Kurozu-treated group, and the solid bar the Kurozu moromimatsu–treated group. Values are means ± SD. $^*P < 0.001$ versus other groups.

Total MMP-9 amounted to 38.2 ± 10.6 ng/mg of protein in the control group and 35.6 ± 8.22 ng/mg of protein in the Kurozu group. However, it was significantly reduced to 21.5 ± 6.1 ng/mg of protein by administration of Kurozu-M ($P < 0.05$ versus control; Fig. 3B). Activated MMP-9 amounted to 1.6 ± 0.5 ng/mg of protein in the control group, 1.4 ± 0.6 ng/mg of protein in the Kurozu group, and 0.7 ± 0.2 ng/mg of protein in the Kurozu-M group ($P < 0.05$ for the Kurozu-M group versus control; Fig. 3B).

Discussion

Our results indicate that the administration of Kurozu-M inhibits the development of colon cancer in human colon cancer cell transplantation model in mice. Further, the administration of Kurozu-M inhibited nitrotyrosine production, decreased total MMP-2 and total MMP-9 levels, and inhibited activation of MMP-2 and MMP-9 in the lesion in this model.

Earlier studies had indicated that extract of Kurozu can inhibit chemical carcinogenesis [3,4,6]. However, in our study, the administration of Kurozu-M inhibited the development of colon cancer in a mouse model, whereas the administration of Kurozu did not prevent tumor growth. The major constituent of Kurozu is acetic acid, whereas the major component of Kurozu-M is a complex mixture of organic materials, including bacterial metabolites. The active components of Kurozu-M remain to be identified.

In this study, we found that administration of Kurozu-M inhibited production of nitrotyrosine in tumor tissue. Nitrotyrosine is generated through two pathways in vivo. One is the peroxynitrite pathway, in which tyrosine reacts with peroxynitrite to afford nitrotyrosine, and the second is the myeloperoxidase pathway, in which tyrosine reacts with myeloperoxidase and nitrite [7,8]. We previously reported that peroxynitrite is produced in human colon cancer tissue [5]. In contrast, myeloperoxidase is localized in polymorphonuclear leukocytes in vivo, but in this study we could not detect any accumulation of polymorphonuclear leukocytes by means of HE staining of cancerous tissue. Therefore, Kurozu-M administration may inhibit the peroxynitrite pathway. Possible mechanisms include inhibition of nitric oxide, superoxide, and/or peroxynitrite production, and scavenging of nitric oxide, superoxide, and/or peroxynitrite. Further work is needed to examine these possibilities.

The administration of Kurozu-M also inhibited MMP-2 and MMP-9 activity in cancerous tissue. These are representative gelatinases that contribute to the distant metastasis of cancer [9], and they are produced by cancer cells or macrophages [10]. A tetradecanoylphorbol acetate-responsive element is present in the promoter region of MMP-9 and is activated by various cytokines, such as interleukin and tumor necrosis factor [11]. In addition, MMP-9 is activated by nuclear factor-κB and MMP-2 [12]. MMP-2 is mainly activated by MT1-MMP, but recently it was shown that peroxynitrite also activates MMP-2 [13,14]. Kurozu-M may have inhibited cancer growth in our model through inhibition of peroxynitrite formation and MMP-2 and MMP-9 activities.

Kurozu moromimatsu was active against Lovo cells in this study, but not against DLD-1 cells. Lovo and DLD-1 cells differ not only in the degree of cellular differentiation but also in the expression of furin, which contributes to MMP activation [15]. The former line originates from well-differentiated adenocarcinoma and expresses furin protein, whereas the latter originates from poorly differentiated adenocarcinoma and does not express furin protein. It would be worth examining whether MMP activity is reduced in the absence of furin.

Conclusion

The administration of Kurozu-M inhibited tumor growth in a Lovo cell–transplanted mouse model and also inhibited nitrotyrosine production and activation of MMP-2 and MMP-9.

References

[1] Shimoji Y, Tamura Y, Nakamura Y, Nanda K, Nishidai S, Nishikawa Y, et al. Isolation and identification of DPPH radical scavenging compounds in Kurosu (Japanese unpolished rice vinegar). J Agric Food Chem 2002;50:6501–3.

[2] Shen X, Falzon M. PTH-related protein enhances LoVo colon cancer cell proliferation, adhesion, and integrin expression. Regul Pept 2005; 125:17–27.

[3] Shimoji Y, Kohno H, Nanda K, Nishikawa Y, Ohigashi H, Uenakai K, et al. Extract of Kurosu, a vinegar from unpolished rice, inhibits azoxymethane-induced colon carcinogenesis in male F344 rats. Nutr Cancer 2004;49:170–3.

[4] Nanda K, Miyoshi N, Nakamura Y, Shimoji Y, Tamura Y, Nishikawa Y, et al. Extract of vinegar "Kurosu" from unpolished rice inhibits the proliferation of human cancer cells. J Exp Clin Cancer Res 2004;23: 69–75.

[5] Szaleczky E, Pronai L, Nakazawa H, Tulassay Z. Evidence of in vivo peroxynitrite formation in patients with colorectal carcinoma, higher plasma nitrate/nitrite levels, and lower protection against oxygen free radicals. J Clin Gastroenterol 2000;30:47–51.

[6] Shimoji Y, Sugie S, Kohno H, Tanaka T, Nanda K, Tamura Y, et al. Extract of vinegar "Kurosu" from unpolished rice inhibits the development of colonic aberrant crypt foci induced by azoxymethane. J Exp Clin Cancer Res 2003;22:591–7.

[7] Eiserich JP, Hristova M, Cross CE, Jones AD, Freeman BA, Halliwell B, et al. Formation of nitric oxide-derived inflammatory oxidants by myeloperoxidase in neutrophils. Nature 1998;391:393–7.

[8] Fukuyama N, Takebayashi Y, Hida M, Ishida H, Ichimori K, Nakazawa H. Clinical evidence of peroxynitrite formation in chronic renal failure patients with septic shock. Free Radic Biol Med 1997; 22:771–4.

[9] Gullu IH, Kurdoglu M, Akalin I. The relation of gelatinase (MMP-2 and -9) expression with distant site metastasis and tumour aggressiveness in colorectal cancer. Br J Cancer 2000;82:249.

[10] Djonov V, Cresto N, Aebersold DM, Burri PH, Altermatt HJ, Hristic M, et al. Tumor cell specific expression of MMP-2 correlates

with tumor vascularisation in breast cancer. Int J Oncol 2002; 21:25–30.

[11] Steinbrenner H, Ramos MC, Stuhlmann D, Mitic D, Sies H, Brenneisen P. Tumor promoter TPA stimulates MMP-9 secretion from human keratinocytes by activation of superoxide-producing NADPH oxidase. Free Radic Res 2005;39:245–53.

[12] Wittrant Y, Theoleyre S, Couillaud S, Dunstan C, Heymann D, Redini F. Relevance of an in vitro osteoclastogenesis system to study receptor activator of NF-kB ligand and osteoprotegerin biological activities. Exp Cell Res 2004;293:292–301.

[13] Munoz-Najar UM, Neurath KM, Vumbaca F, Claffey KP. Hypoxia stimulates breast carcinoma cell invasion through MT1-MMP and MMP-2 activation. Oncogene 2005.

[14] Migita K, Maeda Y, Abiru S, Komori A, Yokoyama T, Takii Y, et al. Peroxynitrite-mediated matrix metalloproteinase-2 activation in human hepatic stellate cells. FEBS Lett 2005;579:3119–25.

[15] Deryugina EI, Ratnikov BI, Yu Q, Baciu PC, Rozanov DV, Strongin AY. Prointegrin maturation follows rapid trafficking and processing of MT1-MMP in Furin-negative colon carcinoma LoVo cells. Traffic 2004;5:627–41.

Basic Res Cardiol 102:209–216 (2007)
DOI 10.1007/s00395-006-0629-9

ORIGINAL CONTRIBUTION

Naoto Fukuyama
Etsuro Tanaka
Yasuhiko Tabata
Hisanori Fujikura
Masao Hagihara
Hiromi Sakamoto
Kiyoshi Ando
Hiroe Nakazawa
Hidezo Mori

Intravenous injection of phagocytes transfected ex vivo with FGF4 DNA/ biodegradable gelatin complex promotes angiogenesis in a rat myocardial ischemia/reperfusion injury model

Received: 18 April 2006
Returned for 1. revision: 21 June 2006
1. Revision received: 11 September 2006
Accepted: 9 October 2006
Published online: 27 October 2006

N. Fukuyama (✉) · H. Fujikura · M. Hagihara · K. Ando · H. Nakazawa
Depts. of Physiology, Internal Medicine and Center for Regenerative Medicine
Tokai University School of Medicine
Isehara, 259-1193, Japan
Tel.: +81-463/93-1121
Fax: +81-463/93-6684
E-Mail: fukuyama@is.icc.u-tokai.ac.jp

E. Tanaka
Dept. of Nutritional Sciences
Tokyo University of Agriculture
Tokyo, Japan

Y. Tabata
Research Center for Biomedical Engineering
Kyoto University
Kyoto, Japan

H. Sakamoto
Genetics Division
National Cancer Center Research Institute
Tokyo, Japan

H. Mori
National Cardiovascular Center Research Institute
Suita, Japan

Abstract Conventional gene therapies still present difficulties due to poor tissue-targeting, invasiveness of delivery, method, or the use of viral vectors. To establish the feasibility of using non-virally ex vivo transfected phagocytes to promote angiogenesis in ischemic myocardium, gene-transfection into isolated phagocytes was performed by culture with positively charged gelatin impregnated with plasmid DNA. A high rate of gene transfection was achieved in rat macrophages and human monocytes, but not in mouse fibroblasts. The efficiency was 68 ± 11 % in rat macrophages and 78 ± 8 % in human monocytes. Intravenously injected phagocytes accumulated predominantly in ischemic tissue (13 ± 8 %) and spleen (84 ± 6 %), but negligibly in other organs in rodents. The efficiency of accumulation in the target ischemic tissue reached more than 86 % on direct local tissue injection. In a rat model of myocardial ischemia-reperfusion, intravenous injection of fibroblast growth factor 4 (FGF4)-gene-transfected macrophages significantly increased regional blood flow in the ischemic myocardium (78 ± 7.1 % in terms of flow ratio of ischemic/non-ischemic myocardium) compared with intravenous administration of saline (36 ± 11 %) or non-transfected macrophages (42 ± 12 %), or intramuscular administration of naked DNA encoding FGF4 (75 ± 18 %). Enhanced angiogenesis in the ischemic tissue we confirmed histologically. Similarly, intravenous injection of FGF4-gene-transfected monocytes enhanced regional blood flow in an ischemic hindlimb model in mice (93 ± 22 %), being superior to the three other treatments described above (38 ± 12, 39 ± 15, and 55 ± 12 %, respectively).

Phagocytes transfected ex vivo with FGF4 DNA/gelatin promoted angiogenesis. This approach might have potential for non-viral angiogenic gene therapy.

Key words angiogenesis – cells – gene therapy – growth substances – ischemia

Abbreviations and acronyms

ANOVA = analysis of variance
FGF4 = fibroblast growth factor-4
GFP = green fluorescent protein
pI = isoelectric point

Introduction

Conventional gene therapies still require improvement with regard to transfection efficiency and safety [1, 2], as well as tissue targeting [3], despite recent advances. Achievement of a high transfection rate often requires a viral vector, but the safety of the viruses has not yet been

Basic Research in Cardiology, Vol. 102, No. 3 (2007)

established [4–6]. Conventional non-viral vectors seem to be inferior to viral ones in transfection efficiency, except for nucleofection [7, 8]. Conventional gene therapy using a viral vector can induce inflammation in the gene-transduced tissue [9]. Moreover, in vivo gene-delivery to the localized target tissue usually necessitates invasive approaches. For example, direct gene-transfection to cardiomyocytes requires surgical operation [10] or cardiac catheterization [11, 12]. On the other hand, ex vivo gene-transfection is less invasive, but tissue-targeting by intravenous injection is difficult to achieve [3].

Macrophages accumulate in ischemic tissue based on the mechanism of immune response (chemotaxis) [13]. This suggests that intravenous transplantation of macrophages may target the ischemic tissue in vivo. Tabata et al. previously reported that gelatin particles are phagocytized by macrophages [14, 15]. The isoelectric point (pI) of gelatin can be changed by modification of its residues, and positively charged gelatin can be impregnated with negatively charged substances [16] such as nucleic acid [17]. Thus, gelatin may be suitable as a vector for transfecting phagocytes ex vivo.

We describe here a study aimed at examining the feasibility of a new concept for less invasive, cell-based gene therapy, by means of ex vivo gene transfection into isolated phagocytes (macrophages and monocytes) using a non-viral vector, gelatin, followed by intravenous injection of the transfected phagocytes. The present method has significant advantages over conventional cell-based gene delivery [18, 19], in that the intravenously injected cells (phagocytes) not only produce protein from the transfected gene, but have a tissue-targeting ability.

Methods

This study was performed in accordance with the Guideline of Tokai University School of Medicine on Animal Use, which conforms to the NIH Guide for the Care and Use of Laboratory Animals (DHEW publication No. (NIH) 86-23, Revised 1985, Offices of Science and Health Reports, DRR/NIH, Bethesda, MD 20205).

Animals

A total of 121 Fisher rats (male, 10 weeks old, Clea Japan Inc., Tokyo) and 61 nude SCID mice (male, 6 weeks old, Shizuoka Animal Center, Shizuoka, Japan) were used. Rats were anesthetized by inhalation of diethyl ether for harvesting macrophages and with isofluren (1.5–3 %) for thoracotomy, after which they were mechanically ventilated with a mixture of oxygen and nitrous oxide. Mice were anesthetized by intraperitoneal injection of sodium pentobarbital (40 mg/kg).

A model of myocardial ischemia-reperfusion injury was prepared in 41 rats. The remaining 80 rats were used for collecting activated macrophages. The heart was exposed via thoracotomy, and the proximal left anterior descending coronary artery was ligated [20] for 180 min, followed by reperfusion. A model of hindlimb ischemia was prepared in 61 mice. The left femoral artery was ligated and resected [21].

Cells

Macrophages were obtained from 80 rats. Thioglycolate (4 %, 8 ml) was injected into the peritoneal cavity, and after 4 days, peritoneal macrophages were collected [22]. Monocytes were obtained from peripheral blood of healthy volunteers. Leukocyte-rich plasma was obtained by dextran 500 sedimentation and layered onto Nycoprep 1.068 (Nycomed, Birmingham, UK). The monocyte-containing layer was aspirated, washed twice and allowed to adhere to the dish for 90 minutes. Fibroblasts (NIH 3T3, Invitrogen Corporation, Carlsbad, CA) were also used. The cells were resuspended in RPMI 1640 medium (Sigma) containing 5 % heat-inactivated fetal calf serum and cultured for 7–14 days. The cell viability and type were determined by trypan blue exclusion and by immunostaining using anti-macrophage antibody up to 14 days.

Genes and vector

Complementary DNA (cDNA) of green fluorescent protein (GFP), Renilla luciferase or human hst1/FGF4 (FGF4) [17] was inserted into the expression vector pRC/CMV (Invitrogen Corporation, Carlsbad, CA) and the constructs were designated as pRC/CMV-GFP, pRC/CMV-luciferase and pRC/CMV-HST1-10, respectively. Preparation and purification of the plasmid from cultures of pRC/CMV-GFP-, pRC/CMV-luciferase-, or pRC/CMV-HST1-10-transformed *Escherichia coli* were performed by equilibrium centrifugation in cesium chloride-ethidium bromide gradients.

Gelatin was prepared from porcine skin [14]. After swelling in water the gelatin particles used in this study were spheroids with a diameter of approximately 5–30 μm, water content of 95 %, and pI of 11. Gelatin (2 mg) was incubated with 50 μg of the plasmid for 7 days at 4 °C to make a gelatin-DNA complex [14].

Experimental protocols

Ex vivo gene transfection Macrophages, monocytes, and fibroblasts (1×10^6) were cultured with the gelatin-DNA complex (2 mg of gelatin plus 50 μg of DNA) for 14 days on a culture dish (100 mm in diameter). Gene ex-

pression of GFP was evaluated by fluorescence microscopy and fluorescence-activated cell sorting. Luciferase activity in the cell lysate was evaluated with a photon counter system after cell lysis [23].

Organ distribution of phagocytes injected intravenously and directly into ischemic muscle To examine tissue-targeting by intravenous injection of transfected phagocytes, the distribution of the cells into organs was evaluated by immunohistochemistry. In the rat model of myocardial ischemia-reperfusion injury, the GFP-gene-transfected macrophages (1.0×10^6 each) were injected into the superficial dorsal vein of the penis at the initiation of reperfusion (n = 7 and 5, respectively). In the mouse model of hindlimb ischemia, the GFP-gene-transfected monocytes (1.0×10^6) were injected into the caudal vein 14 days after induction of ischemia (n = 5). To examine the tissue-targeting by direct local injection of transfected phagocytes, the distribution of the cells into organs was also evaluated. In the rat model of myocardial ischemia-reperfusion injury (n = 7) and the mouse model of hindlimb ischemia (n = 5), the same numbers of transfected macrophages and monocytes were directly injected into ischemic myocardium and ischemic skeletal muscle, respectively. Tissue samples were obtained 24 hours after cell administration. Each tissue was homogenized and cytospin was performed. Immunohistochemical analysis was done with anti-GFP antibody (CLONTECH, USA. GFP-monoclonal antibody). GFP positive macrophages were counted in each tissue and expressed as a percentage of total GFP-positive cells.

Amelioration of ischemia by intravenous injection of angiogenic gene-transfected phagocytes The angiogenic effect of intravenously injected FGF4-gene-transfected phagocytes on the ischemia models was evaluated. In the rat model of myocardial ischemia-reperfusion injury, FGF4-gene-transfected macrophages (n = 5), non-transfected macrophages (1.0×10^6 each) (n = 5), or saline (n = 5) were injected into the superficial dorsal vein of the penis, or naked FGF4-DNA (50 μg) was injected directly into the ischemic myocardium (n = 5), at the initiation of reperfusion. Fourteen days after the cell administration, blood flows in the ischemic and non-ischemic regions in the heart were evaluated with a noncontact laser Doppler flowmeter (FLO-N1, Omegawave Corporation). Then, tissue samples were obtained and histological analysis was performed. In a mouse model of hindlimb ischemia, just after induction of ischemia, FGF4-gene-transfected monocytes (n = 15), non-transfected monocytes (n = 8) (1.0×10^6 each), or saline (n = 10) were injected into the caudal vein, or naked FGF4-DNA (50 μg) was injected directly into the ischemic muscle (n = 12). Fourteen days after induction of ischemia, blood flows in the limbs were evaluated with the noncontact laser Doppler flowmeter (FLO-N1, Omegawave Corporation).

Histology

Ten micrometer sections were cut from formalin-fixed, paraffin-embedded tissue. Two sections were used for H.E. staining and azan staining, and eight sections were used for immunohistochemical staining. Immunohistochemical staining was performed by an indirect immunoperoxidase method. Anti-GFP antibody, anti-Mac1 antibody (BMA Biomedicals Ag, Switzerland), and anti-CD31 antibody (Serotec, UK) were used as primary antibodies. Mac1-antigen is specific to macrophages/monocytes. Anti-Ig, peroxidase-linked species-specific F(ab')2 fragments (Amersham Pharmacia Biotech UK Ltd., UK), were used as a secondary antibody. Double staining was performed with alkaline staining and peroxidase staining. The vessel density stained with von Willebrand factor-antibody was calculated by morphometric assessment in one 16 randomly selected fields of each heart and expressed as number/mm^2.

Statistical analysis

Data are presented as mean values ± SD. Differences were assessed by using ANOVA (analysis of variance) with the Scheffe's multiple comparisons test. A value of $P < 0.05$ was considered statistically significant.

Results

Ex vivo gene transfection

We studied whether genes could be transfected into isolated rat macrophages, human monocytes, and mouse fibroblasts ex vivo by using gelatin. Transfection of the GFP gene into isolated rat macrophages (Figs. 1A and B) and human monocytes (Figs. 1C and D), but not into mouse fibroblasts (data not shown), was achieved by culture with gelatin-DNA complex for 14 days. The gene transfection efficiency into rat macrophages was 68 ± 11% (30 experiments, Fig. 2A) and that into human monocytes was 78 ± 8% (30 experiments) as determined with a fluorescence activated cell sorter. Sequential analysis after luciferase-gene transfection into rat macrophages revealed high expression after 14 days of culture (Fig. 2B).